

# Effect of initial surface finish on effectiveness of shot peening treatment using enhanced periodic cell model

Fan Yang · Zhuo Chen · S. A. Meguid

Received: 14 July 2014 / Accepted: 5 August 2014 / Published online: 24 October 2014  
© Springer Science+Business Media Dordrecht 2014

**Abstract** In this paper, we investigate the effect of the initial surface finish of the target on shot peening effectiveness using realistic 3D finite element simulations. Specifically, a large number of random shot impingements were simulated using an enhanced periodic cell model. The target material which is made from TI-6Al-4V is assumed to be strain-rate sensitive and follows the kinematic hardening law. ABAQUS/PYTHON scripts were developed to average the peening residual stresses at each depth of the target, and to calculate the corresponding surface roughness. The simulation was validated by comparing the results with the published work in literature. The periodicity of the model was also examined and verified. The model is further used to investigate the effect of the initial surface roughness on the effectiveness of the shot-peening treatment. The evolutions of the residual stress, plastic strain and the surface morphology during the peening process have all been investigated and the results discussed. The work reveals that a rough surface finish can lead to major reduction in the effectiveness of the shot peening treatment in terms of the generation of the highly beneficial compressive residual stresses.

**Keywords** Shot peening · Surface finish · Periodic cell model · Finite element · Random shots

## 1 Introduction

Shot peening is a cold-working treatment widely used to improve the fatigue life of metallic components by introducing compressive residual stresses to the near-surface layer of the components. It is accomplished by bombarding the surface of the component with small spherical shots at a relatively high impinging velocity (Meguid 1986; Schulze 2006). During the peening process, a layer of compressive residual stress is generated near the peened surface due to the inhomogeneous elasto-plastic deformation during indenting and rebounding of impinging shots (Kobayashi et al. 1998). This compressive residual stress is beneficial for retarding crack initiation and propagation (Hammond and Meguid 1990). Therefore, shot peening is a very useful treatment to enhance the fatigue resistance and prolong the service life of critical components in aerospace and automobile industry.

The effectiveness of shot peening relies on three aspects: intensity, coverage and surface roughness. In view of its importance, a number of efforts have been devoted to investigate the effectiveness of shot peening. Li et al. (1991), Bhuvanaraghan et al. (2010) sought analytical approaches to predict the compressive residual stress field. Some efforts were made on experiments,

---

F. Yang · Z. Chen · S. A. Meguid (✉)  
Mechanics and Aerospace Design Laboratory, University  
of Toronto, 5 King's College Road, Toronto,  
ON M5S 3G8, Canada  
e-mail: meguid@mie.utoronto.ca

including the contributions made by Al-Hassani (1981), Kobayashi et al. (1998), Noyan and Cohen (1985), Foss et al. (2013), Torres and Voorwald (2002), among others. The hole-drilling method (Nobre et al. 2000; Chaudhuri et al. 1994) and X-ray diffraction method (Noyan and Cohen 1985; Foss et al. 2013; Prevey 1991) were used to measure peening residual stress. These methods were supplemented by numerical techniques such as the finite element method. Schiffner et al. (1999) used an axisymmetric model to investigate the effects of shot velocity, diameter and material parameters on the residual stress distribution. Meguid et al. (1999a, b, 2007) used symmetry cell models to investigate the effects of shot velocity, size, shape and inter-space upon the development of plastic zone and residual stress. Hong et al. (2008a, b) simulated the oblique incidence of a single shot on a large plate and investigated the effect of initial yielding and strain-hardening properties of targets. Kim et al. (2013) modeled the shots as rigid, elastic and elastoplastic balls respectively and examined the effect of different shot models on peening residual stresses. Multiple impingements were also simulated. Klemenz et al. (2009) modeled 121 rigid shots impinging at the target in a specified order with full coverage. Mylonas and Labeas (2011), and Sheng et al. (2012) investigated random shot impingements.

Despite the extensive work in literature, there are still some issues that need to be addressed. For example, for the material properties of the target, some authors used rate insensitive models (Meguid et al. 1999a; Frija et al. 2006; Edberg et al. 1995). Others considered strain rate sensitivity in their constitutive models (Kim et al. 2013; Mylonas and Labeas 2011; Meguid et al. 2002). The results of Meguid et al. (2002) showed that the strain rate sensitivity of the target material cannot be neglected for modeling high speed impact. Another issue for the material model is concerned with the use of isotropic hardening law; see, e.g., Hong et al. (2008a) and Meguid et al. (2002). This is appropriate when only single or a few shots are simulated. However, when a large number of continuous impingements are modeled, the target material will experience multiple loading–unloading and reverse loading cycles. For materials which harden or soften with cyclic loading, the Bauschinger effect becomes dominant. For this situation, kinematic hardening law is more appropriate than the isotropic hardening law (Klemenz et al. 2009; Mylonas and Labeas 2011). Therefore, in this study a strain rate

sensitive material with kinematic hardening law is used to model the target material.

In real shot peening treatment, the shots are randomly projected onto the target. Meguid et al. (2002, 2007), Schiffner et al. (1999), and Majzoubi et al. (2005) developed symmetry cell models using symmetry boundary conditions to model the effect of adjacent shots. However, the symmetry models are not suitable to model the random impingements. This is because the shots usually impinge at several positions such as the corner, the center and the edge midpoint in the symmetry cell models. Difficulties will arise when the shot impinges at a general location, especially near the cell boundaries. Mylonas and Labeas (2011) used a confined cell with fixed boundaries to model the random shot impingement. In their models, the shots impinged at a confined area at the center of the cell surrounded by marginal region. The marginal region was used to reduce the influence of the boundary conditions. However, it is difficult to determine an appropriate range for the marginal region. Therefore, a new periodic cell model is developed in this study to model the random impingements of a large number of shots.

Another issue in the current shot peening research is that the target surface is always assumed to be initially smooth. While in real practice, the surface of target inevitably has an initial roughness. The initial roughness may be induced in the casting or the cold-working processes (Davim 2010). Recently, some authors also recommended the two-stage shot peening (Ahmad and Crouch 1989; Park and Jung 2002) or re-shot-peening treatment (Jiang et al. 2007) to optimize the beneficial residual stresses. The two-stage shot peening is composed of a first peening treatment with relative large shots followed by a second treatment with smaller shots. The first peening treatment will impart a rough initial surface for the second peening process. Therefore, it is of practical importance to investigate the effect of the initial roughness on the shot peening effectiveness. So far, studies on the initial roughness for shot peening are quite limited. The only effort that we have found was made by Sheng et al. (2012) who investigated the influence of initial surface roughness on the generated residual stress profile beneath the indentation location. The compressive zone depth was found to be smaller for a rougher surface. It is therefore the purpose of this paper to systematically investigate the influence of initial surface roughness on the effectiveness of the shot peening treatment.

This paper is organized as follows. Following this introduction, Sect. 2 presents the proposed periodic model for random impingements and gives some necessary validations. Section 3 investigates the evolution of peening residual stress, plastic deformation and surface morphology as the number of shots increases. Sections 4 and 5 investigate the effect of the initial surface roughness and the effect of shot size on the obtained results, respectively. In Sect. 6, we conclude the paper.

## 2 A new periodic finite element model

### 2.1 Geometry, discretization and boundary condition of the FE model

The three-dimensional FE model was developed using the commercial code ABAQUS version 6.11 (2011). The explicit solver was adopted to calculate the dynamic response. The idea is to simulate a large region by calculating a small representative cell, as depicted in Fig. 1a. The shots are assumed to impinge the target in multiple arrays. In each array, the shots are close to each other to maximize peening coverage. The size of the

representative computational cell is  $2R \times 2R \times H$ , as shown in Fig. 1b. Where,  $R$  is the shot radius. The height of the cell  $H$  was taken as  $5R$ , since this value is large enough to neglect the bottom boundary influence (Meguid et al. 2002). Fixed boundary condition was applied to all the nodes on the bottom boundary. The coordinate system was created with the origin being at the center of the target surface and z-axis along the normal of the surface.

A periodic cell model was developed in our previous work (Yang et al. 2013). In that model, the periodic boundary conditions were applied to the opposite side boundaries of the cell, to couple the corresponding degrees of freedom (DOFs). In this paper, the periodic cell model is further complemented in order to simulate the random impingements of a large number of shots. The difficulty is that when the impinging position is close to the boundary of the cell, the contact region may extend beyond the cell boundary, i.e., the shot would get into contact with the target surface that is not included in the computational cell. To overcome this difficulty, a new method is developed in which additional shots are included in the model when the impinging position of the investigated shot is close to the cell boundaries. The additional shots are periodic images of the original shot,

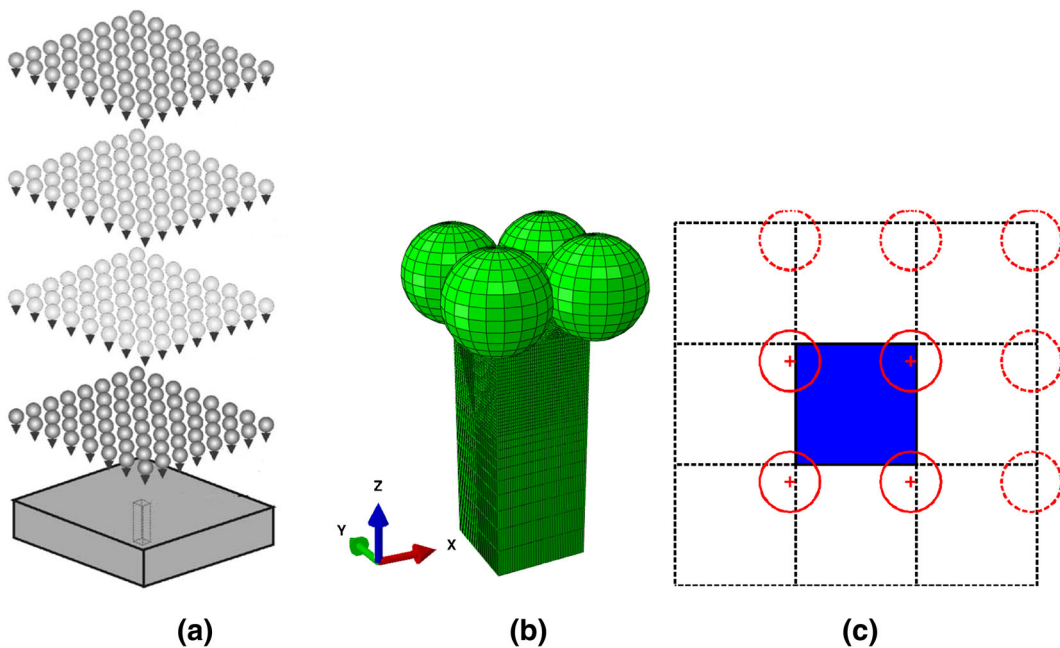


**Fig. 1** The new periodic cell model. **a** Illustration of the simulated scenario and the representative cell. **b** Discretized FE model. **c** Top view of the simulated shot and its periodic images.

The blue region indicates the calculated target cell, the red circles indicate the contact regions of each shot. (Color figure online)

and serve only to model the contact between the original shot and the target surface that is beyond the boundaries of the computational cell. Therefore, the additional shots have zero mass and rotary inertia, and their DOFs are fully coupled to the original shot. Figure 1b, c show an example of the periodic cell model. The original shot impinges at an arbitrary position, which is close to the upper-right corner of the cell target. Therefore, its three periodic images are included in the model to correctly simulate the contact between the shots and the target.

The target cell was discretized using eight-noded solid elements with reduced integration scheme. The reduced integration scheme was chosen because the results showed no discernable difference from those using fully integration scheme, and the computation time was largely reduced. The mesh was refined near the top surface. Mesh convergence tests were conducted and the final element size was chosen around  $0.05R$  for the top region of the target. The shots were modeled as rigid spheres of radius  $R = 0.5$  mm and impinging velocity  $V = 50$  m/s, unless otherwise specified. This velocity value was also used by Kim et al. (2013) and would thus allow comparisons with the earlier works. The rigid shots were implemented in the FE model using an analytical rigid surface with an equivalent point mass and an equivalent point rotational inertia positioned at its centre. A typical model contained 92,428 elements and took about 45 h to simulate 5 ms on a 2.6 GHz computer processor.

## 2.2 Material models

The material models used by Meguid et al. (2007) were applied in this paper. The target was chosen as Ti-6Al-4V alloy which is widely used in aerospace industry. The material parameters were as follows: Young's modulus  $E = 114$  GPa, Poisson's ratio  $\nu = 0.342$ , density  $\rho = 4430$  kg/m<sup>3</sup> and initial yield stress  $\sigma_y = 827$  MPa. The kinematic hardening law was applied, since it is more suitable for the cyclic loading condition in shot peening of cyclic dependent behaviour target materials, such as Ti-6Al-4V alloy (Peirs et al. 2012). The yield surface can be expressed as,

$$\sqrt{\frac{3}{2}(\boldsymbol{\sigma}' - \boldsymbol{\alpha}') : (\boldsymbol{\sigma}' - \boldsymbol{\alpha}')} = \sigma_0 \quad (1)$$

where,  $\boldsymbol{\sigma}$  and  $\boldsymbol{\alpha}$  are respectively the stress tensor and back stress tensor with prime indicating the deviatoric

parts,  $\sigma_0$  is the equivalent stress defining the size of the yield surface.  $\sigma_0$  is dependent on the strain rate to account for strain-rate sensitivity. The evolution of the back stress can be given as,

$$\dot{\boldsymbol{\alpha}} = C \frac{1}{\sigma_0} (\boldsymbol{\sigma} - \boldsymbol{\alpha}) \dot{\boldsymbol{\varepsilon}}^{\text{pl}} - \gamma \boldsymbol{\alpha} \dot{\boldsymbol{\varepsilon}}^{\text{pl}} \quad (2)$$

with

$$\bar{\boldsymbol{\varepsilon}}^{\text{pl}} = \int_0^t \sqrt{\frac{2}{3} \boldsymbol{\varepsilon}^{\text{pl}} : \boldsymbol{\varepsilon}^{\text{pl}}} dt \quad (3)$$

where  $\bar{\boldsymbol{\varepsilon}}^{\text{pl}}$  is the effective plastic strain defined in Eq. 3,  $\boldsymbol{\varepsilon}^{\text{pl}}$  is the tensor of plastic strain rate,  $C$  and  $\gamma$  are two constants. The constants  $C$  and  $\gamma$  can be determined by quasi-static uniaxial stress–strain data (Meguid et al. 2007). From Eq. 2, the uniaxial stress–strain relation can be written as:

$$\sigma = \frac{C}{\gamma} \left( 1 - e^{-\gamma \bar{\boldsymbol{\varepsilon}}^{\text{pl}}} \right) + \sigma_0 \quad (4)$$

For the kinematic hardening condition, the size of the yield surface  $\sigma_0$  is kept constant as the initial yielding stress  $\sigma_y$ . Therefore,  $C$  and  $\gamma$  can be fitted from the uniaxial stress–strain curve using Eq. 4. The fitted parameters are  $C = 1$ . Pa and  $\gamma = 9.33$ . The rate dependence of  $\sigma_0$  can be determined using the data of Premack and Douglas [38], which was also used for the rate sensitivity of the isotropic hardening model described by Meguid et al. (2007). To compare the kinematic hardening law and the isotropic hardening law, a uniaxial cyclic loading case was investigated. The loading history profile is shown in Fig. 2a. The stress–strain curves are plotted in Fig. 2b, c for the isotropic hardening and the kinematic hardening models, respectively. The mismatch in the loading and the unloading curves for cycles other than the first in Fig. 2b is caused by the strain rate sensitivity of the material model. Without strain rate sensitivity, the isotropic hardening model can only lead to coincident loading and unloading curves following the first cycle. On the other hand, the kinematic hardening model can well depict the hysteresis loop.

The material for the rigid shots was steel with density  $\rho_{\text{shot}} = 7850$  kg/m<sup>3</sup>. The interfacial friction coefficient for the contact between the shots and the target was assumed to be 0.3. According to Kim et al. (2013) and Meguid et al. (2002), a friction coefficient larger than 0.2 will make no much difference for the

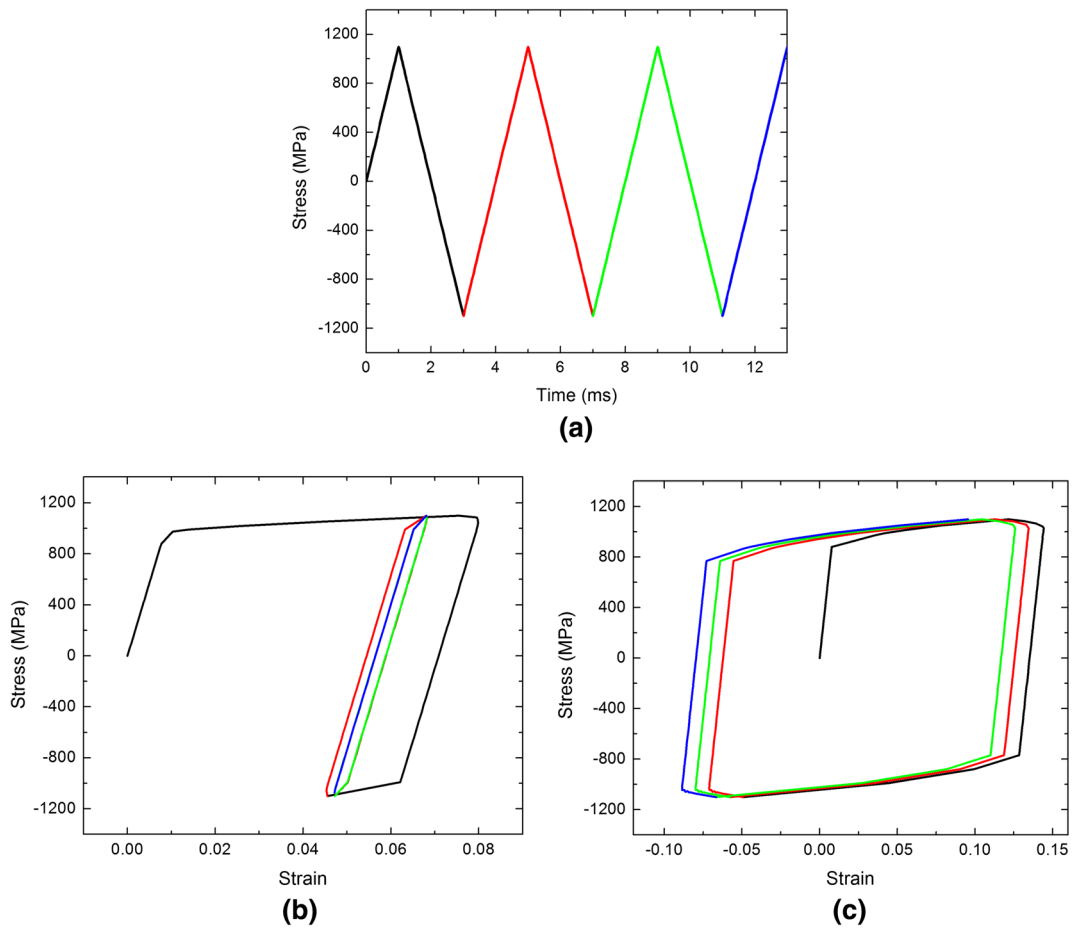


**Fig. 2** Comparison between the isotropic hardening law and the kinematic hardening law for cyclic loading with different colors indicating different cycles: **a** history profile of the load,

**b** stress–strain curves following isotropic hardening law, and **c** stress–strain curves following kinematic hardening law

residual stress results. The respective material damping parameters were chosen as  $\alpha = \frac{1}{H} \sqrt{\frac{2E}{\rho}}$  and  $\beta = 2 \times 10^{-9}$  s for the mass proportional and stiffness proportional components (Meguid et al. 2002). The interval between sequential shots  $t_{\text{int}}$  was selected as 4  $\mu$ s so that the oscillation due to one shot impingement can be largely damped before the impingement of next shot.

### 2.3 Validation of the model

In order to validate the periodicity of the new model, three simulations were carried out with one shot impinging at different locations: the center, the corner and an arbitrary location. Figure 3 depicts the impinging locations and the contact region for the three

simulations in one graph. The contact area is obtained from the zero contact stress contour line at the largest indentation moment. Figure 4a compares the residual stress profile beneath the impinging location between the three simulations. The stress profiles for different impinging locations match well with each other. Figure 4b compares the displacement histories of the incident shot for the three simulation cases. Again, the shot displacement results for different impinging locations match well with each other. These consistencies provide a validation for the periodicity in the model.

In order to validate our simulations, we compared our results from the new periodic model with existing work in literature. The work by Meguid et al. (2007), who used a symmetry cell model was taken for this comparison. For this purpose, we used exactly the

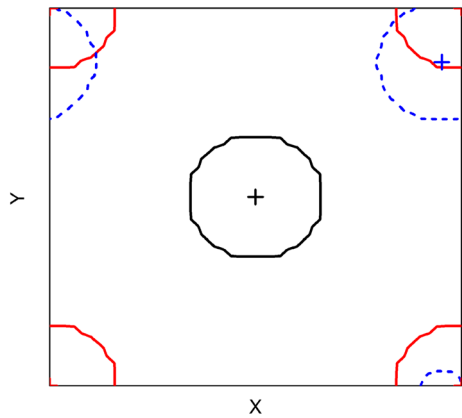


**Fig. 3** Top view depicting the impinging locations for the three simulations, with the contour lines indicating the obtained contact regions

same geometry, material and impinging velocity as those used by Meguid et al. (2007). The periodic cell is fourfold as large as the symmetry cell used by Meguid et al. (2007). Four series of multiple impingements were simulated. Each series includes four arrays of shots impinging sequentially at the target surface. The locations of the impingements in each series are depicted in the top views in Fig. 5 for the two models. The numbers in Fig. 5 indicate the impinging sequence. Our final peening residual stress distributions along the depth beneath the four locations are compared with those in Meguid et al. (2007) in Fig. 6. The comparison reveals excellent agreement with the results of Meguid et al. (2007) which used symmetry cell model. It is also worth noting that that a different commercial code LS-DYNA was used by Meguid et al. (2007).

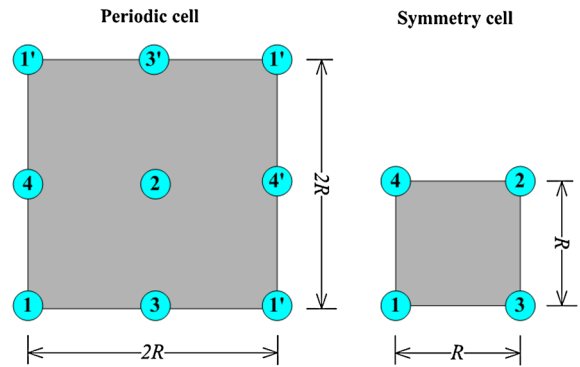


**Fig. 5** Top views of the periodic model and the reproduced symmetry model (Meguid et al. 2007). The numbers indicate the impinging sequence of the shots. The numbers with prime indicate the shots are periodic images

### 3 Peening treatment of smooth surfaces

We firstly investigate the evolution of the peening residual stresses, plastic strains and the resulting surface roughness of a smooth target using the proposed periodic cell model. In order to realize random impingements, a large number of shots were initially placed above the target with positions following Eq. 5.

$$\begin{aligned}
 x_i &= r_x(i)L_x \\
 y_i &= r_y(i)L_y \\
 z_i &= i \cdot t_{int}V
 \end{aligned}
 \tag{5}$$

where,  $r_x(i)$  and  $r_y(i)$  are random numbers in range [0, 1],  $t_{int}$  is the time interval between two adjacent impingements, as stated in Sect. 2.2. The shots were assigned the same initial velocities, and impinged the

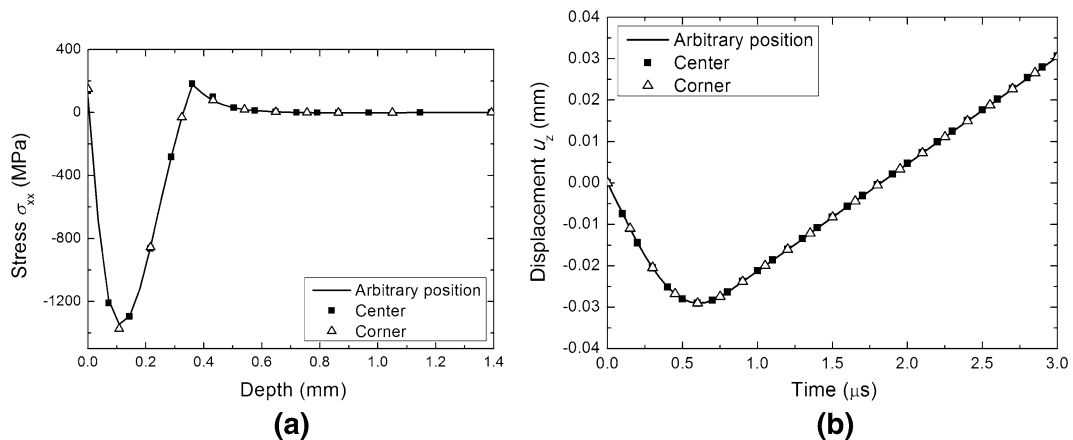


**Fig. 4** Comparison of **a** the peening residual stress profile, and **b** the shot displacement history for different impinging locations

**Fig. 6** Comparison of the present results, using the new periodic cell model, with those by Meguid et al. (2007) using symmetry cell model for the residual stress profiles at the four locations indicated in the right graph. The *solid lines* indicate our present results, and the *dots* indicate the results published in literature (Meguid et al. 2007)

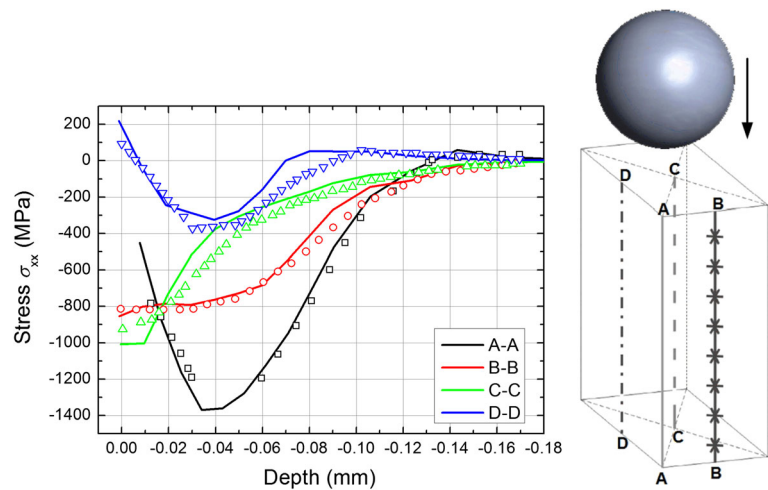
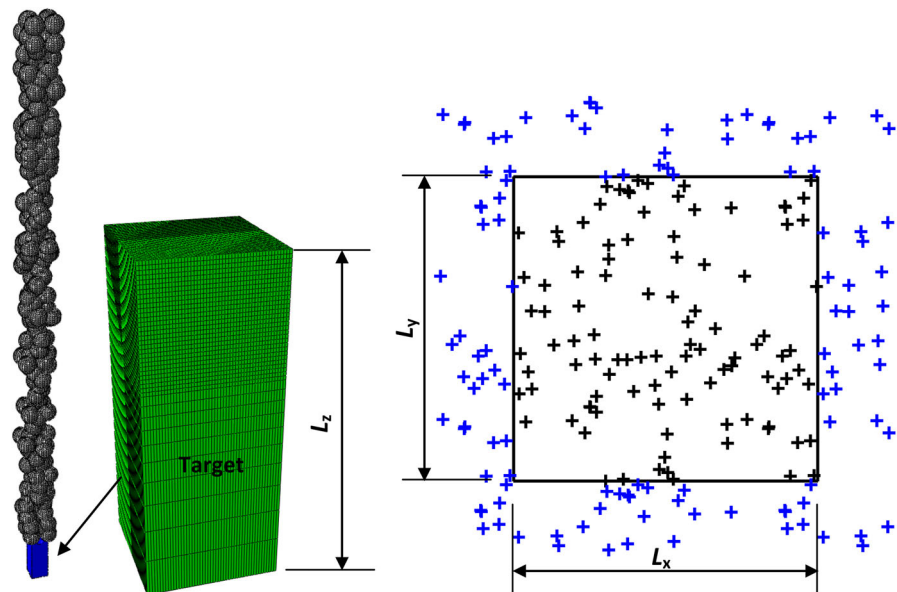


**Fig. 7** Illustration of random impingement model. The dots indicate the impinging locations of the random shots (*black*) as well as their periodic images (*blue*). (Color figure online)



target one by one in a sequence depending on their initial distances from the target surface. In this study, 100 impingements were simulated with the impinging positions indicated in Fig. 7. The dimensions of the simulation cell were  $L_x = L_y = 1$  mm,  $L_z = 2.5$  mm.

Firstly, the residual stress was investigated. The residual stress  $\sigma_{xx}$  was averaged across the  $xy$ -plane at each depth. An ABAQUS/PYTHON script was developed to conduct these calculations. Figure 8a shows the average residual stress  $\sigma_{xx}$  versus depth for different number of impinging shots. It indicates that both the magnitude of the induced residual stresses and the compressed layer increase with the increase in

the shot numbers. The stress profile finally converges to a steady state after repeated bombardments of shots. Figure 8b shows the root mean square (RMS) deviation of the residual stress  $\sigma_{xx}$  relative to its average value versus the depth for different number of impinging shots. It shows that the deviation of residual stress decreases with the increase in the shot numbers. The sharp increase of the relative deviation at a certain depth is due to the fact that the average residual stress  $\sigma_{xx}$  becomes near zero beyond that depth. The evolution of the residual stress fields can be clearly seen in the contour plots in Fig. 9. As it shows, the distribution of the residual stress became more

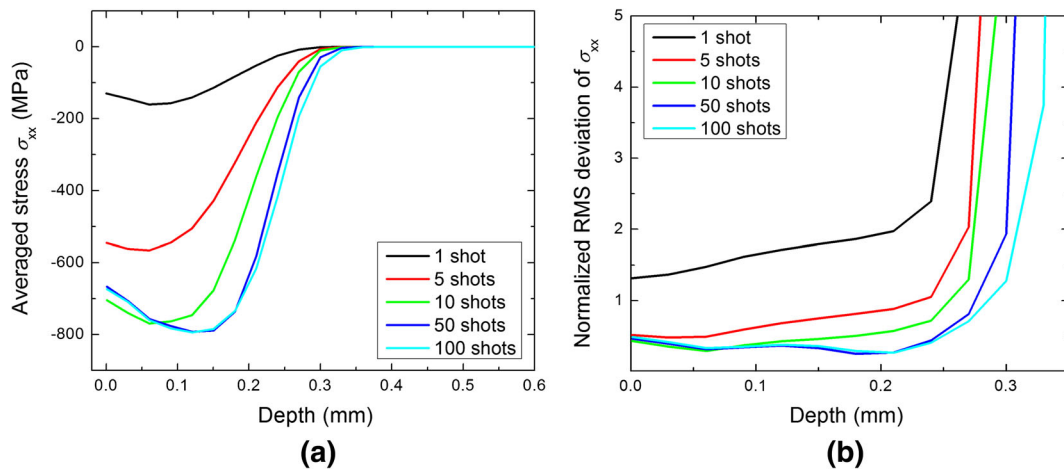


**Fig. 8** Residual stress distribution for different number of impinging shots: **a** average residual stress  $\sigma_{xx}$  versus depth, **b** relative deviation of residual  $\sigma_{xx}$  from its average value versus depth

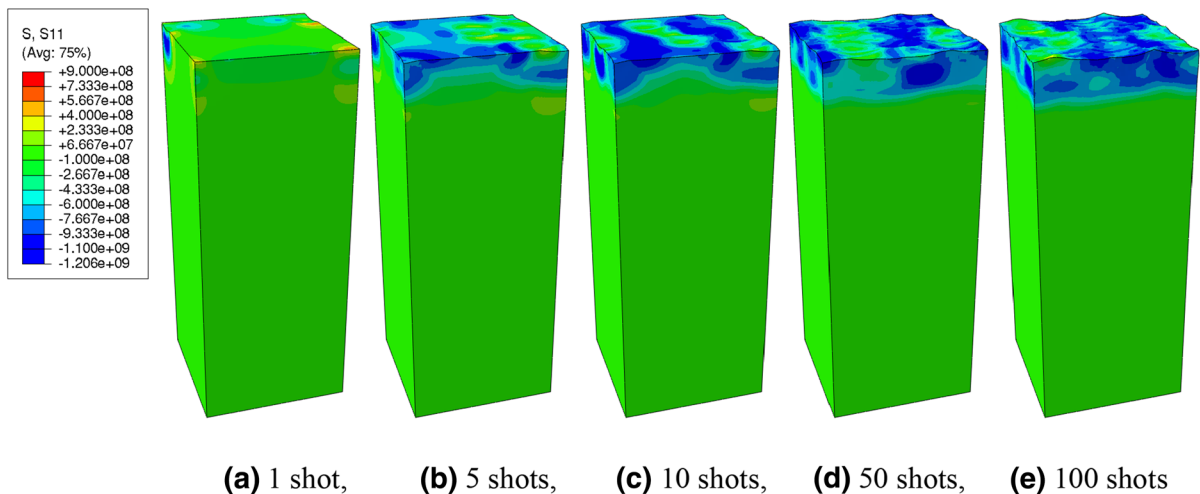


**Fig. 9** Evolution of the residual stress distribution  $\sigma_{xx}$  as the number of impinging shots increases. **a** 1 shot, **b** 5 shots, **c** 10 shots, **d** 50 shots, **e** 100 shots

uniform and the compressive zone became enlarged as the shot number increased.

Secondly, the effective plastic strain was investigated. An ABAQUS/PYTHON script was developed to average the effective plastic strain  $\bar{\epsilon}^{pl}$  across the xy-plane at each depth. Figure 10a shows the averaged  $\bar{\epsilon}^{pl}$  versus depth for different number of impinging shots. It shows that  $\bar{\epsilon}^{pl}$  increases with the accumulative number of impingements. Unlike the residual stress field, the  $\bar{\epsilon}^{pl}$  profile does not converge with the increase in the current number of shots. This is because the target material experiences substantial reverse

plasticity in each loading–unloading–reloading cycle due to repeated shot peening as shown in Fig. 2c. Comparing Fig. 10a with Fig. 8a, one observes that the size of plastic zone is a little smaller than the size of the compressed layers. Figure 10b shows the profile of relative RMS deviation of  $\bar{\epsilon}^{pl}$  from its average value for different number of impinging shots. It shows that the deviation of  $\bar{\epsilon}^{pl}$  decreases as the number of shots increases. Figure 11 shows the evolution of the distribution of  $\bar{\epsilon}^{pl}$  as the number of shots increases. It clearly shows that the  $\bar{\epsilon}^{pl}$  increases with the number of impinging shots. Also, the plastic strain became more



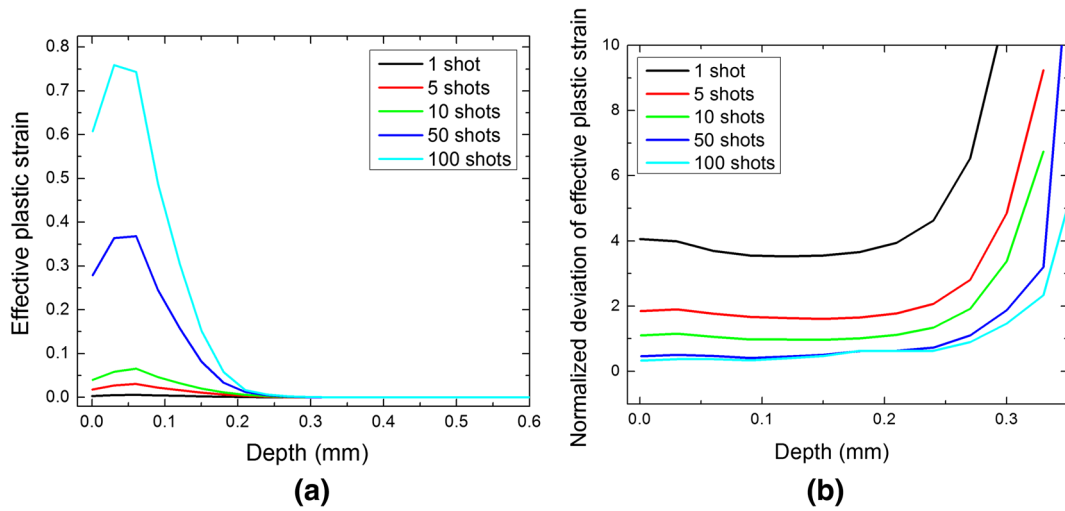


**Fig. 10** Distribution of effective plastic strain for different number of impinging shots. **a** Averaged  $\bar{\epsilon}^{pl}$  versus depth. **b** Relative deviation of  $\bar{\epsilon}^{pl}$  from its average value versus target depth

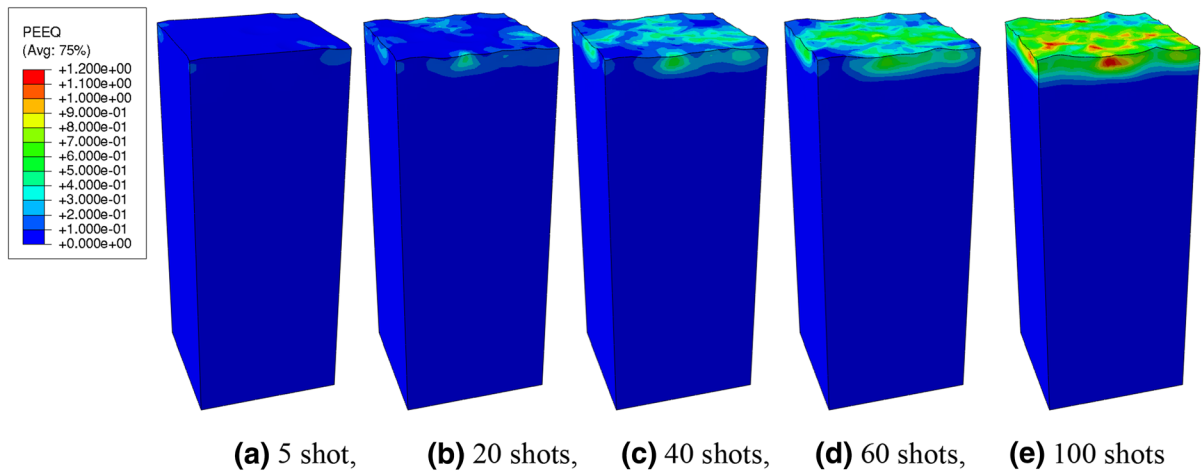


**Fig. 11** Evolution of the distribution of effective plastic strain  $\bar{\epsilon}^{pl}$  as the accumulative number of shots increases. **a** 5 shot, **b** 20 shots, **c** 40 shots, **d** 60 shots, **e** 100 shots

uniformly distributed as the number of impinging shots increased.

Thirdly, the surface morphology was investigated. The roughness was assessed using two definitions: the arithmetic type  $R_a$  and root mean square type  $R_{rms}$ , as defined in Eq. 6 below:

$$R_a = \frac{1}{N} \sum_{i=1}^N |y_i|, \quad R_{rms} = \sqrt{\frac{1}{N} \sum_{i=1}^N y_i^2} \quad (6)$$

where,  $y_i$  ( $i = 1, 2, \dots, n$ ) is the vertical deviation of the  $i$ th point from the mean plane of the surface profile,  $N$  is the number of points calculated. Figure 12 plots the surface roughness versus the accumulative mass of impinging shots. It indicates that the surface roughness is increased as the shot peening continued until an asymptotic value is reached. The asymptotic value is about  $5.5 \mu\text{m}$  for  $R_a$ , and  $7 \mu\text{m}$  for  $R_{rms}$  for the given impact energy. Figure 13 plots the surface profiles for

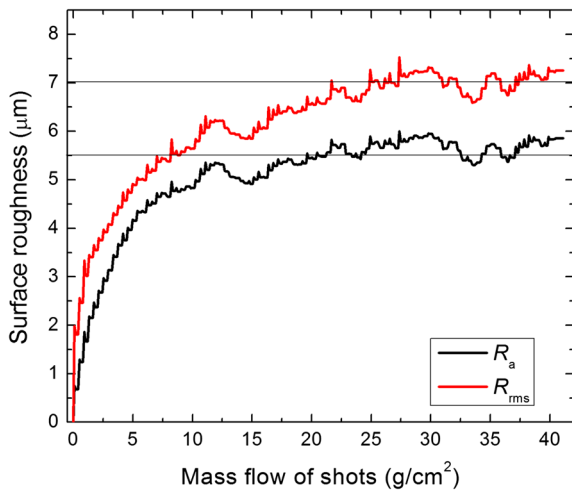


**Fig. 12** Surface roughness versus accumulative mass of the impinging shots. The guide lines indicate the asymptotic values of the surface roughness

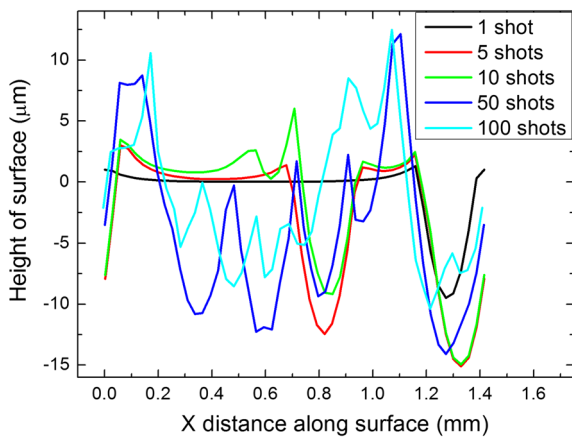


**Fig. 13** Evolution of surface profiles as the number of impinging shots increases

different number of impinging shots. It shows that the surface became more asperous with increased exposure time.

One interesting question is whether we can obtain consistent results when the random number is generated differently. In order to answer this question, three simulations with different random shot generation were carried out. The average residual stress profiles from the three simulations are compared in Fig. 14. The comparisons are made after 5 and 100 shot impingements, respectively. The results reveal insignificant variance between different random shot generations, especially after a large number of shot

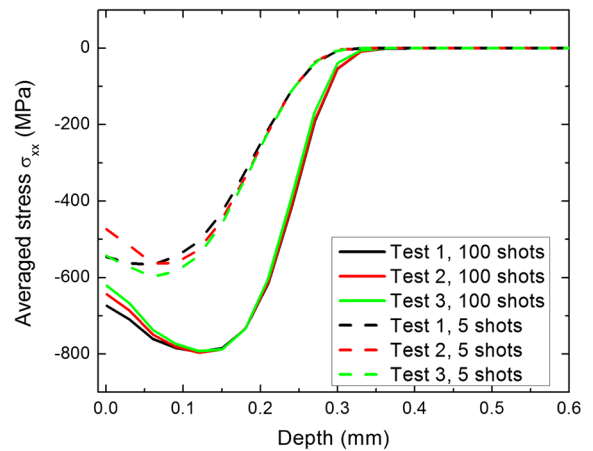


**Fig. 14** Comparison of the average residual stress profiles between three trial runs with different random shot generation

impingements. Therefore, the effect of different generation of random shots is neglected in this work.

We further examined the effect of strain hardening laws of the target material model on the obtained residual stress field. Figure 15 compares the average residual stress profiles from the isotropic hardening model with those from the kinematic hardening model. that the figure shows that after 1 shot impingement, the stress profiles from the two models coincide with each other. While after 100 shot impingements, the difference becomes distinct. Therefore, it is felt that the kinematic hardening model is more appropriate for modeling the cyclic loading condition in shot peening process.

#### 4 Peening treatment of rough surfaces

Next, we investigate the effect of the initial surface roughness upon the resulting residual stress field, the plastic strain field and surface roughness. The morphology of the surface is assumed to follow a bi-sinusoidal function, as in Eq. 7.

$$z = z_{amp} \cos\left(\frac{2n\pi}{L_x}x\right) \cos\left(\frac{2n\pi}{L_y}y\right) \tag{7}$$

where  $z_{amp}$  is the amplitude of the sinusoidal surface profile,  $n$  is a natural number. The mesh was generated using TRUEGRID version 2.1. Five simulations of target samples with different initial roughnesses were generated, as shown in Fig. 16. In these configurations, the ratio of the amplitude to the wavelength of

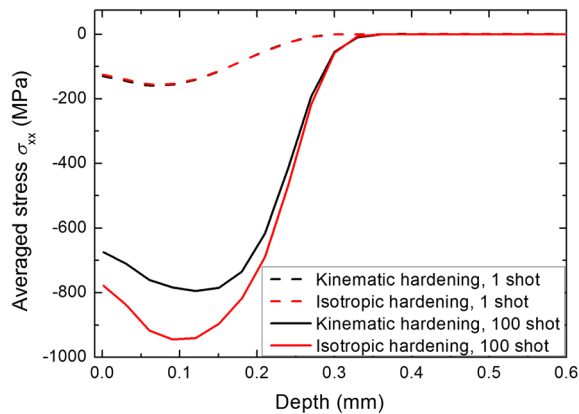


**Fig. 15** Comparison of the average residual stress profiles from the isotropic hardening model with those from the kinematic hardening model

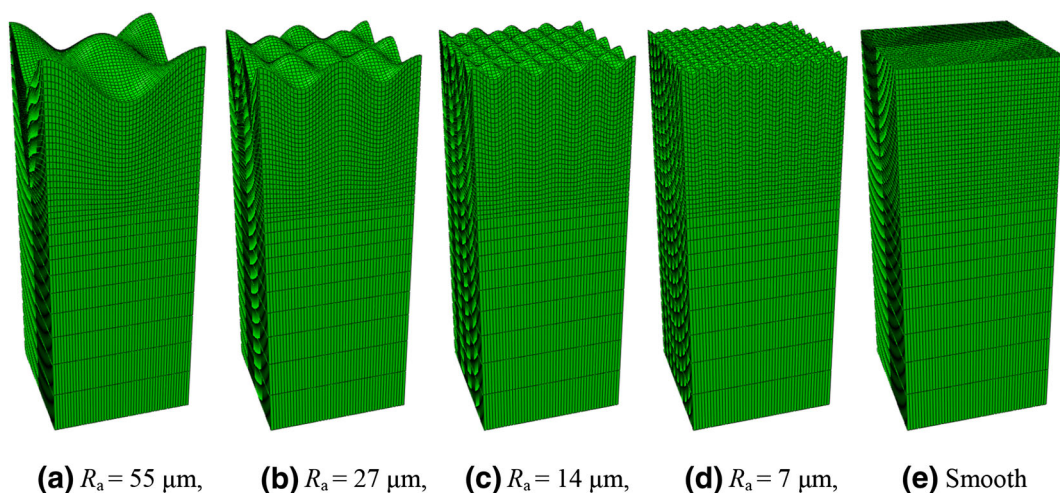
the sinusoidal surface profile was kept constant as 0.15, according to the experimental observations by Jiang et al. (2007). Therefore,  $n z_{\text{amp}}/L_x = 0.15$ .

Figure 17 depicts the distribution of the residual stress  $\sigma_{xx}$  along target thickness after 100 shot impingements for different initial surface roughnesses. Figure 17a depicts the profile of the average residual stress. It indicates that both the magnitude and the size of the compressed layer decrease with the increase in the initial target roughness. It also shows that the average residual stress is nearly zero for the largest initial roughness investigated ( $R_a = 55 \mu\text{m}$ ).

Figure 17b shows the deviation of the residual stress from its average value at each depth. It indicates that the deviation is larger for a rougher surface, especially at the target surface. For example, in the case where the initial roughness of the surface is  $55 \mu\text{m}$ , the largest residual stress deviation is 600 MPa, while if the initial roughness is less than  $7 \mu\text{m}$ , the largest deviation is only around 300 MPa. These results indicate that a rough initial surface can result in major reductions in the induced residual stress field and consequently the effectiveness of shot peening treatment in terms of the residual stress generation.

Next, our attention is focused on the plastic strain. Figure 18a, b respectively plot the profiles of the average value and the RMS deviation from the average value for the effective plastic strain  $\bar{\epsilon}^{\text{pl}}$  versus depth for different initial surface roughnesses. Figure 18a shows that the depth of the plastic zone decreases as the initial roughness increases. For a large initial roughness, maximum  $\bar{\epsilon}^{\text{pl}}$  takes place at the surface. While for a small initial roughness, maximum  $\bar{\epsilon}^{\text{pl}}$  takes place at a certain depth beneath the surface. The magnitude of  $\bar{\epsilon}^{\text{pl}}$  at surface increases as the initial roughness increases. Figure 18b indicates that the distribution of  $\bar{\epsilon}^{\text{pl}}$  is more nonuniform for a rougher target, especially at surface.

The evolution of surface morphology was also investigated. Figure 19 shows the variation of the surface roughness  $R_a$  with the accumulative shot mass



**Fig. 16** FE simulation samples with different initial surface roughnesses. **a**  $R_a = 55 \mu\text{m}$ , **b**  $R_a = 27 \mu\text{m}$ , **c**  $R_a = 14 \mu\text{m}$ , **d**  $R_a = 7 \mu\text{m}$ , **e** Smooth

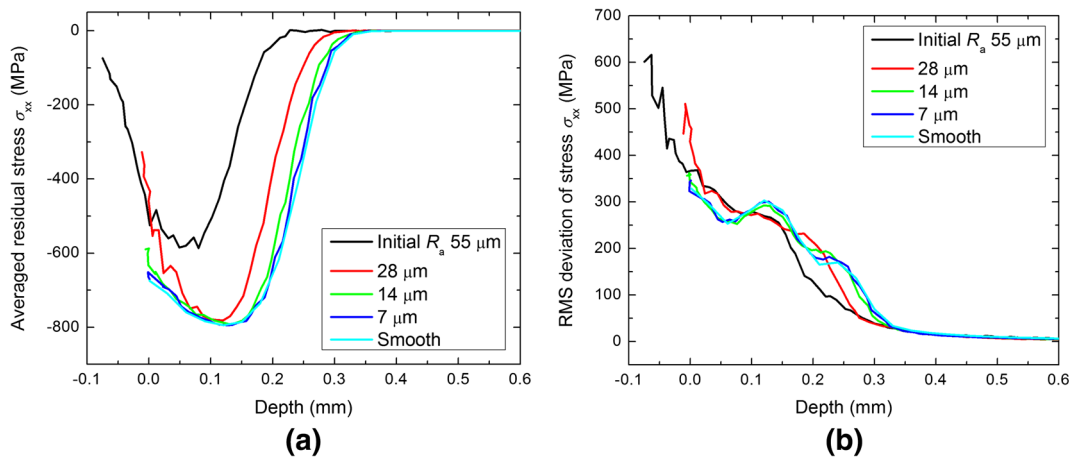


**Fig. 17** Residual stress distribution after 100 shot impingements for targets with varied surface finish: **a** average residual stress  $\sigma_{xx}$  versus target depth, **b** RMS deviation of residual  $\sigma_{xx}$  from its average values

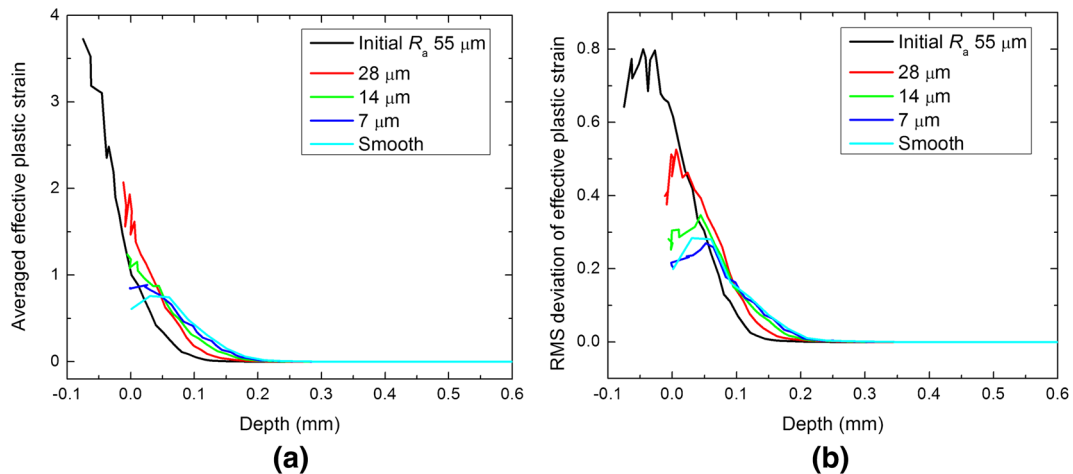


**Fig. 18** Distribution of effective plastic strain  $\bar{\epsilon}^{pl}$  after 100 shot impingements for different initial surface finish: **a** averaged  $\bar{\epsilon}^{pl}$  versus target depth, **b** deviation of  $\bar{\epsilon}^{pl}$  from its average value versus depth

for targets of different initial roughnesses. It indicates that the surface roughness  $R_a$  decreases during the shot peening treatment for all the investigated targets except the smooth one, for which  $R_a$  increases. It is interesting to find that for the targets with initial roughness less than 14  $\mu\text{m}$ ,  $R_a$  converges to a similar value around 5.5  $\mu\text{m}$  after considerable exposure to shot impingements. Figure 20 depicts the final surface morphology with displacement contours for the five investigated targets. It clearly shows that a rougher initial surface results in larger displacement fields at the surface. Figure 21 shows evolution of the surface

profile during the peening treatment for the rough target with initial  $R_a$  of 55  $\mu\text{m}$ . It reveals that the waviness amplitude of the surface profile for the rough target decreases as the number of shot impingements increases. This tendency is different from the case of the smooth target shown in Fig. 14.

## 5 Effect of shot size

Next, we turn our attention to the shot size. Three shot radii: 0.5, 0.625 and 0.75 mm were investigated. The

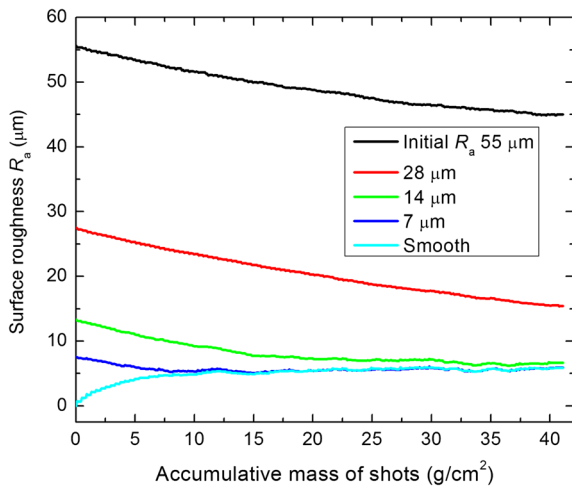


**Fig. 19** History curves of the surface roughness  $R_a$  for targets with different initial roughnesses

results from initially rough surfaces were compared with those of initially smooth surfaces for each shot size. For the rough surface finish, the initial roughness and wavelength were kept constant. The initial  $R_a$  is selected as  $14\ \mu\text{m}$  for all cases. The larger shot size

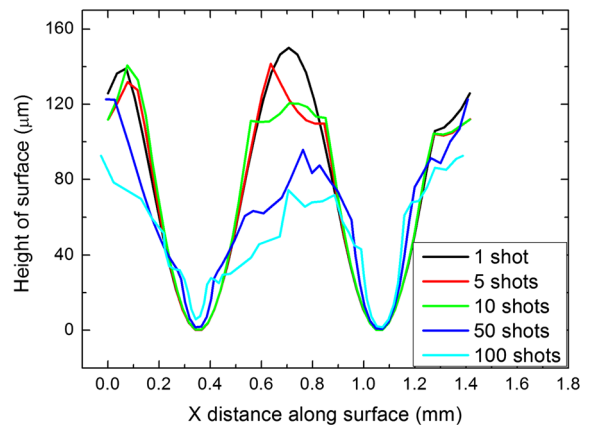


**Fig. 21** Evolution of surface profiles for the roughest target for different number of shot impingements

corresponded to the larger model dimensions, and more surface wavinesses. The three created rough target samples are shown in Fig. 22. The obtained profiles of the average residual stress  $\sigma_{xx}$  versus depth from these simulation cases are compared in Fig. 23. It shows that the magnitude of the residual stress does not differ much for different size of shots, while the

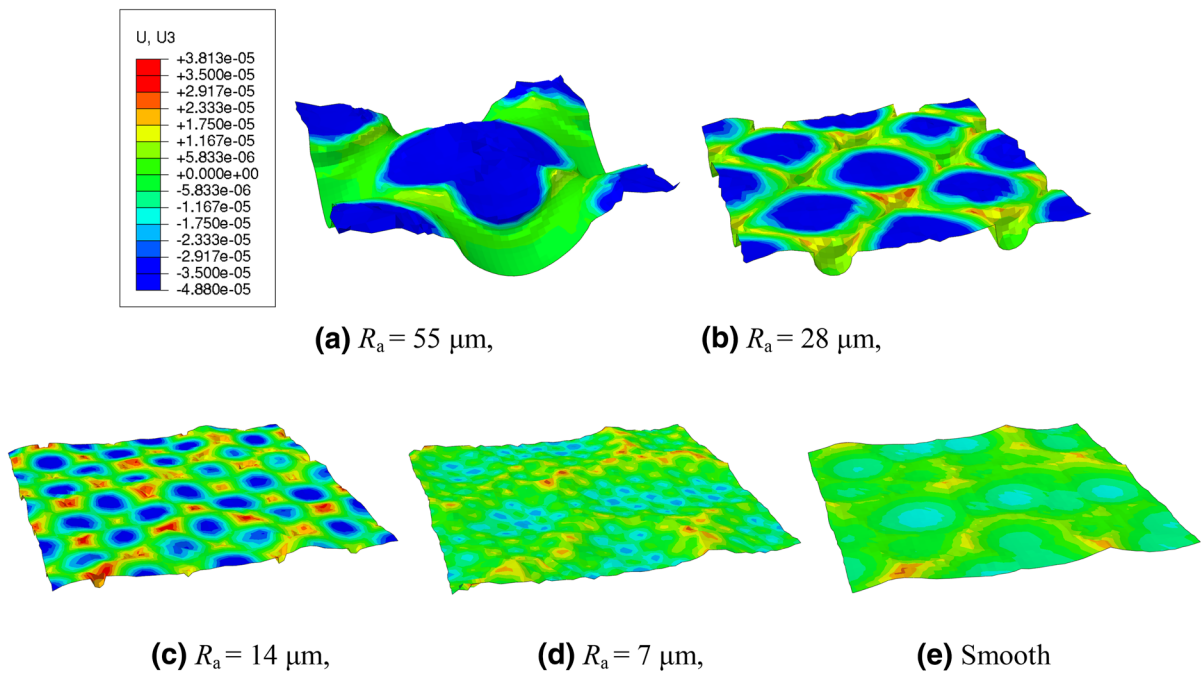


**Fig. 20** The final surface morphology with displacement contours for targets with different initial roughnesses. **a**  $R_a = 55\ \mu\text{m}$ , **b**  $R_a = 28\ \mu\text{m}$ , **c**  $R_a = 14\ \mu\text{m}$ , **d**  $R_a = 7\ \mu\text{m}$ , **e** smooth

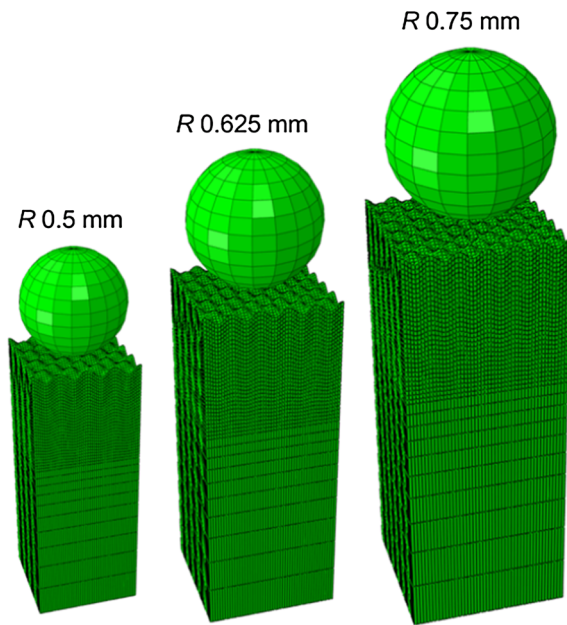


**Fig. 22** Three rough target samples for different sizes of shots

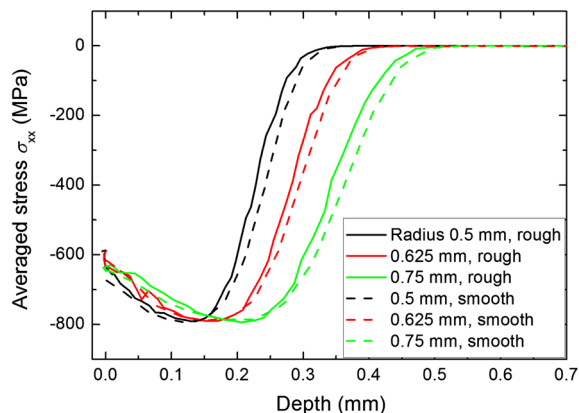


**Fig. 23** Profiles of average residual stress  $\sigma_{xx}$  for different shot size and different initial surface finish

depth of compressed layer increases somewhat linearly with the shot diameter. These tendencies hold for both the rough and the smooth targets. For the same shot size, the smooth target has larger compressed layer than the rough target. Figure 24 plots the history curves of surface roughness for the investigated cases. It is interesting to note that after considerable exposure of peening in our simulations, the surface roughness  $R_a$  will converge to an asymptotic value. This asymptotic value depends on the shot size, with larger shots resulting in larger final surface roughness.

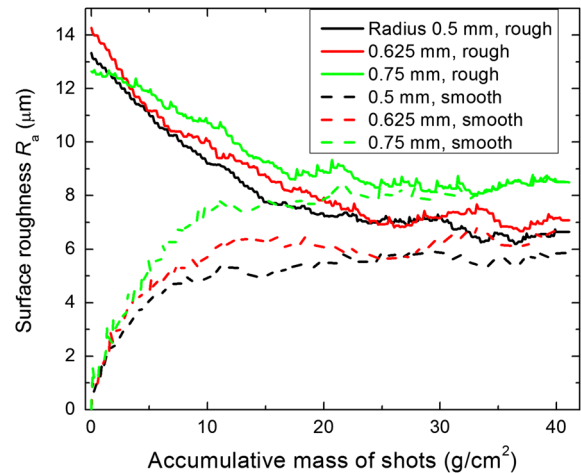


**Fig. 24** History curves of surface roughnesses for different shot size and different initial surface finish

## 6 Conclusions

In this paper, realistic three dimensional FE simulations are carried out to study the effect of the initial surface roughness of the treated targets on the effectiveness of the shot peening treatment. The results of our work reveal the following:

1. An enhanced elasto-plastic periodic cell model, that makes use of kinematic hardening and accounts for strain rate sensitivity, was successfully developed and used to implement random shot impingements in the peening treatment of surfaces with varied roughness,
2. Both the magnitude and the depth of the compressive residual stress field increase with the increase in the number of impinging shots. The residual stress converges to asymptotic value after considerable exposure of shot impingement.
3. The effective plastic strain increases with the increase in the number of impinging shots. The relative deviation of effective plastic strain from its average value decreases as the peening exposure time increases.
4. Both the magnitude and the range of the compressive residual stress field decrease with the increase in the initial surface roughness of the exposed surface layers. A rough surface finish undermines the effectiveness of the shot peening treatment in terms of the generation of the compressive residual stresses.

5. The surface roughness  $R_a$  will converge to an asymptotic value after considerable exposure of shot impingement.

## References

- Abaqus Analysis User's Manual, version 6.11. Dassault Systèmes Simulia Corp., Providence, RI (2011)
- Ahmad, A., Crouch, E.D.: Dual shot peening to maximize beneficial residual stresses in carburized steels. In: Krauss, G. (ed.) *Carburizing: Processing and Performance: Proceedings of an International Conference*, pp. 277–281. ASM international, Materials Park (1989)
- Al-Hassani, S.T.S.: Mechanical aspects of residual stress development in shot peening. In: *Proceedings of ICSP-1*, Paris, p. 583–602 (1981)
- Bhuvanaraghavan, B., Srinivasan, S.M., Maffeo, B., Prakash, O.: Analytical solution for single and multiple impacts with strain-rate effects for shot peening. *Comput. Model. Eng. Sci.* **57**, 137–158 (2010)
- Chaudhuri, J., Donley, B.S., Gondhalekar, V., Patni, K.M.: The effect of hole drilling on fatigue and residual stress properties of shot-peened aluminum panels. *J. Mater. Eng. Perform.* **3**, 726–733 (1994)
- Davim, J.P.: *Surface Integrity in Machining*. Springer, Berlin (2010)
- Edberg, J., Lindgren, L., Ken-Ichiro, M.: Shot peening simulated by two different finite element formulations. In: Shen, S.F., Dawson, P. (eds.) *Simulation of Materials Processing: Theory, Methods and Applications*, pp. 425–430. Balkema Publishers, Rotterdam (1995)
- Frija, M., Hassine, T., Fathallah, R., Bouraoui, C., Dogui, A.: Finite element modelling of shot peening process: prediction of the compressive residual stresses, the plastic deformations and the surface integrity. *Mat. Sci. Eng. A* **426**, 173–180 (2006)
- Foss, B.J., Gray, S., Hardy, M.C., Stekovic, S., McPhail, D.S., Shollock, B.A.: Analysis of shot-peening and residual stress relaxation in the nickel-based superalloy RR1000. *Acta Mater.* **61**, 2548–2559 (2013)
- Hammond, D.W., Meguid, S.A.: Crack propagation in the presence of shot peening residual stresses. *Eng. Fract. Mech.* **37**, 373–387 (1990)
- Hong, T., Ooi, J.Y., Shaw, B.A.: A numerical study of the residual stress pattern from single shot impacting on a metallic component. *Adv. Eng. Softw.* **39**, 743–756 (2008a)
- Hong, T., Ooi, J.Y., Shaw, B.: A numerical simulation to relate the shot peening parameters to the induced residual stresses. *Eng. Fail. Anal.* **15**, 1097–1110 (2008b)
- Jiang, X.P., Man, C.S., Shepard, M.J., Zhai, T.: Effects of shot-peening and re-shot-peening on four-point bend fatigue behavior of Ti–6Al–4V. *Mater. Sci. Eng. A* **468**, 137–143 (2007)
- Kim, T., Lee, H., Hyun, H., Jung, S.: Effects of Rayleigh damping, friction and rate-dependency on 3D residual stress simulation of angled shot peening. *Mater. Design* **46**, 26–37 (2013)
- Klemen, M., Schulze, V., Rohr, I., Lohe, D.: Application of the FEM for the prediction of the surface layer characteristics after shot peening. *J. Mater. Process. Tech.* **209**, 4093–4102 (2009)
- Kobayashi, M., Matsui, T., Murakami, Y.: Mechanism of creation of compressive residual stress by shot peening. *Int. J. Fatigue* **20**, 351–357 (1998)
- Li, A.K., Yao, M., Wang, D., Wang, R.: Mechanical approach to the residual stress field induced by shot-peening. *Mater. Sci. Eng. A* **147**, 167–173 (1991)
- Majzoubi, G.H., Azizi, R., Alavi Nia, A.: A three-dimensional simulation of shot peening process using multiple shot impacts. *J. Mater. Process. Technol.* **164**, 1226–1234 (2005)
- Meguid, S.A.: *Impact Surface Treatment*. Elsevier Applied Science, Amsterdam (1986)
- Meguid, S.A., Shagal, G., Stranart, J.C.: 3D FE analysis of peening of strain-rate sensitive materials using multiple impingement model. *Int. J. Impact Eng* **27**, 119–134 (2002)
- Meguid, S.A., Shagal, G., Stranart, J.C., Daly, J.: Three-dimensional dynamic finite element analysis of shot-peening induced residual stresses. *Finite Elements Anal. Des.* **31**, 179–191 (1999a)
- Meguid, S.A., Shagal, G., Stranart, J.C.: Finite element modelling of shot-peening residual stresses. *J. Mater. Process. Tech.* **92**, 401–404 (1999b)
- Meguid, S.A., Shagal, G., Stranart, J.C.: Development and validation of novel FE models for 3D analysis of peening of strain-rate sensitive materials. *J. Eng. Mater. Tech.* **129**, 271–283 (2007)
- Mylonas, G.I., Labeas, G.: Numerical modelling of shot peening process and corresponding products: residual stress, surface roughness and cold work prediction. *Surf. Coat. Tech.* **205**, 4480–4494 (2011)
- Noyan, I.C., Cohen, J.B.: An X-ray diffraction study of the residual stress-strain distributions in shot-peened two-phase brass. *Mater. Sci. Eng.* **75**, 179–193 (1985)
- Nobre, J.P., Kornmeier, M., Dias, A.M., Scholtes, B.: Use of the hole-drilling method for measuring residual stresses in highly stressed shot-peened surfaces. *Exp. Mech.* **40**, 289–297 (2000)
- Park, K.D., Jung, C.G.: The effect of compressive residual stresses of two-stage shot peening for fatigue strength of spring steel. In: *Proceedings of the 12<sup>th</sup> International Off-shore and Polar Engineering Conference Kitakyushu, Japan, May 26–31*, pp. 220–223 (2002)
- Peirs, J., Verleysen, P., Degrieck, J.: Study of the dynamic Bauschinger effect in Ti–6Al4V by torsion experiments. *EPJ Web of Conferences* **26**, 01023 (2012). doi:[10.1051/epjconf/20122601023](https://doi.org/10.1051/epjconf/20122601023)
- Premack, T., Douglas, A.S.: Three-dimensional analysis of the impact fracture of 4340 steel. *Int. J. Solids Struct.* **32**, 2793–2812 (1995)
- Prevey, P.S.: X-ray diffraction characterization of residual stresses produced by shot peening. In: Eckersley, J.S., Champagne, J. (eds.) *Shot Peening—Theory and Applications*, pp. 81–93. IITT-International, Gournay-sur-Marne (1991)
- Schiffner, K., Droste gen. Helling, C.: Simulation of residual stresses by shot peening. *Comput. Struct.* **72**, 329–340 (1999)

- Schulze, V.: *Modern Mechanical Surface Treatment*. Wiley-VCH, Weinheim (2006)
- Sheng, X.F., Xia, Q.X., Cheng, X.Q., Lin, L.S.: Residual stress field induced by shot peening based on random-shots for 7075 aluminum alloy. *Trans. Nonferrous Met. Soc. China* **22**, s261–s267 (2012)
- Torres, M.A.S., Voorwald, H.J.C.: An evaluation of shot peening, residual stress and stress relaxation on the fatigue life of AISI 4340 steel. *Int. J. Fatigue* **24**, 877–886 (2002)
- Yang, F., Chen, Z., Meguid, S.A.: 3D FE modeling of oblique shot peening using a new periodic cell. *Int. J. Mech. Mater. Des.* **10**, 133–144 (2013)